Journal of Applied Polymer Science

Enhancement of Polylactide Nucleation by Montmorillonites Intercalated with a Green Seaweed Byproduct

Fabrizio Fordiani,[1] Thierry Aubry,[2] Isabelle Pillin,[2] Yves Grohens[2]

[1]Olmix, Research Division, ZA du Haut Bois, 56580 Bréhan, France

[2]Laboratoire d'Ingénierie des Matériaux de Bretagne (LIMATB), Université de Bretagne Sud, Centre de Recherche, Rue St Maudé, BP 92116, 56321 Lorient Cedex, France

Correspondence to: Y. Grohens (E-mail: yves.grohens@univ-ubs.fr.)

ABSTRACT: Polylactide (PLA) nanocomposites with improved mechanical and barrier properties are of growing industrial interest and therefore required green modified montmorillonites (gm-MMTs) to meet the expectation of totally biosourced material. In this study, ulvans that are polysaccharides and glycoproteins extracted from seaweed are used as surfactants to achieve intercalated clays. The effect of this gm-MMT (ALL350) on the crystallization kinetics of PLA was compared to Cloisite 30B, and pristine MMT was taken as a reference. Rheology, differential scanning calorimetry, and transmission electronic microscopy experiments were performed to better understand the effects that dominate the so-called nucleating effect observed in PLA nanocomposites. It was found that two major driving forces explain the efficiency of the ALL350 that enhances PLA nucleation. The first one is the decrease of the interfacial energy and the second is a reduction of the complex viscosity that acts on the induction period. Reduction of both the interfacial energy and the surface friction forces between PLA chains and polysaccharides-treated clay platelets is assumed to facilitate the induction process. © 2012 Wiley Periodicals, Inc. J. Appl. Polym. Sci. 000: 000–000, 2012

KEYWORDS: PLLA; nanocomposites; crystallization; rheology; nucleation; polysaccharides

Received 3 November 2011; accepted 12 April 2012; published online
DOI: 10.1002/app.37864

INTRODUCTION

The dwindling of fossil resources and the protection of environment for future generations have urged the development of materials synthesized from renewable resources with the possibility of being recyclable or biodegradable.[1,2]

Because of its biodegradability and biocompatibility, use of polylactide (PLA) has expanded rapidly in packaging and biomedical application. However, the ultimate physical properties of polymers, such as their resistance to mechanical impact, the development of crazes, barrier properties, or optical properties, are highly dependent on the morphology of the polymer and, therefore, the crystalline size. The morphology and particularly the degree of crystallinity also influence the hydrolytic degradation kinetics.[3,4] Thus, it is of the utter importance to control the crystallization process to reach specific end uses.

One of the main cost-efficient methods to enhance the physical properties of polymeric materials is the addition of fillers known to act as nucleating agents. The impact of traditional nucleating agents as well as nanofillers used to improve the mechanical property and permeability of polymers have been investigated for poly(L-lactic acid) (PLLA). It turns out that talc[5,6] poly(D-lactic acid) (PDLA) or the stereocomplex crystallites formed upon the addition of PDLA[7,8] mesolactide,[9] dendritic hyperbranched polymer,[10] can effectively promote the nucleation of PLLA. Nam et al.[11] reported that nucleation rate of PLLA is slightly enhanced by natural clay, whereas reduced by organoclay. Moreover, the addition of organoclays shows a tendency to reduce slightly the growth rate and the overall crystallization rate, and it does not affect spherulite sizes.[12] Krikorian and Pochan[13] claimed that the use of two commercial organoclays, Cloisite 15A and 30B, intercalated with alkyl chains with a different surface tension, dictates the extent of dispersion in the final nanocomposites. They reported that the more compatible organoclays, Cloisite 30B (C30B), lead to fully exfoliated nanocomposites, whereas the less compatible Cloisite 15A leads to intercalated systems. An interesting unexplained outcome is the relation between the dispersion and the nucleated ability of organically modified clays. In the case of exfoliated nanocomposites, the low nucleating efficiency behavior coupled with a higher spherulite radial growth rate lead to a greater final spherulite sizes. In contrast, in the case of intercalated nanocomposites, clay acts as an effective

nucleating agent, resulting in a finer morphology and a higher crystalline content compared with the fully exfoliated system.[14]

Commonly, low-cost natural polymers are used as additives to reduce the overall material cost and the environmental impact. Numerous studies have been carried out for PLLA–polysaccharides blends.[15–17] Interestingly, chitosan, a polysaccharide of marine origin, has been used to improve the chemical compatibility between PLLA and layered silicate clay.[18] Recently, Tsuji et al. equally reported the effects of various polysaccharides on the overall PLLA crystallization.[19] It is thus interesting to clarify the effect involved in the enhancement of the PLLA crystallization by polysaccharides.

To tackle this issue, we focused our attention on a complex containing ulvan and glycoproteins extracted from green seaweeds, as a potential additive of PLLA. In this article, we study the impact of montmorillonite (MMT) clay intercalated with ulvan–glycoprotein complex. One of the main advantages in using this complex, for the nanocomposites intercalation, is the use of water as a solvent. Moreover, the exploitation of this marine biomass byproduct can also represent a "green solution" to related environmental and economical concerns. Furthermore, PLLA filled with C30B and pristine MMT are used as reference nanocomposites.

BACKGROUND

Several theories were described to explain crystal growth into polymers. The adjacent re-entry chain-folded model is the most probable mechanism of crystalline block on crystalline lamellae.[20] One classical way of describing data inherited from the crystallization of small entities and originally proposed simultaneously by Johnson and Melh,[21] Avrami,[22–24] and Kolmogorov[25] and usually cited as the Avrami model. Assuming a distribution of initial nuclei already contained in the melt state and conditions for their growth, this model gives the mass crystalline fraction, transformed with the elapsed time according to:

$$\alpha(t) = 1 - \exp(-E), \tag{1}$$

where $\alpha(t) = \frac{\Delta H(t)}{\Delta H_\infty}$, $\Delta H(t)$ and ΔH_∞ represent the overall crystalline enthalpy at a given time t and at an infinite time, respectively. E is the number of activated centers within a sphere of radius $R(t) = Gt$, where G and t stand for the linear growth rate and time, respectively. In the hypothesis of a heterogeneous nucleation, valid for our study, and for crystalline entities with an n dimensional growth, Avrami's law is usually written as follows:

$$\alpha(t) = 1 - \exp(-Kt^n) \tag{2}$$

with the parameter K depends on the growth geometry (factor C), the growth rate $G(T)$, and the nucleation rate N.

The half crystallization time, $t_{1/2}$, for which half the crystallization is achieved, is a characteristic time that relates the overall crystallization to the linear growth rate according to eq. (3):

$$\frac{1}{t_{1/2}} = \left(\frac{CN}{Ln2}\right)^{1/n} G. \tag{3}$$

This relation points out that the overall crystallization rate scales as the linear growth rate $G(T)$ and the nucleation rate N.

Crystal nucleation and crystal growth data are equally often analyzed with a classical thermodynamic approach, which defines the critical size nucleus must have so that the reduction in energy caused by its formation is sufficient to overcome the excess energy associated to the creation of surfaces. The development of this approach has led to the classical nucleation theory of Turnbull and Fisher,[26] which describes the growth of new crystals from a preexisting surface and to the secondary nucleation controlled crystal growth model proposed by Lauritzen and Hoffman[27] to account for the polymer crystallization.

The nucleation rate can be expressed as follows:

$$N(T) = N_0 \exp\left(-\frac{U^*}{R(T - T_0)}\right) \exp\left(-\frac{16\sigma\sigma_e\Delta\sigma(T_m^0)^2}{k\Delta T^2\,\Delta H_m^2}\right), \tag{4}$$

where σ and σ_e stand for the lateral and the folded surface energy, respectively; $\Delta\sigma$ the interfacial energy; and ΔH_m and T_m^0 are the melting enthalpy and the melting temperature of a crystal of an infinite size, respectively. U^* is the transport activation energy and T_0 a reference temperature lower than the glass transition temperature by 30–40 K, below which any motions ceases.

The general form of the growth rate equation is as follows:

$$G = G_0 \exp\left(\frac{-U^*}{R(T - T_0)}\right) \exp\left(-\frac{K_g}{T\Delta T}\right), \tag{5}$$

where K_g is the nucleation constant defined as $K_g = \frac{nb_0\sigma\sigma_e T_m^0}{k\Delta H_m}$, n is an integer that reflects the relative rate of two competing processes: secondary nucleation and surface spreading, and b_0 represents the thickness of a monomolecular nuclei.

Three regimes of crystal growth can be distinguished as a function of the crystallization temperature. Regimes I and II were proposed in 1975[28] and regime III in 1983.[20] Regimes I (low undercoolings) and III (high undercoolings) correspond to kinetics controlled by the secondary germination ($n = 4$), whereas regime II corresponds to competition between secondary and tertiary germination ($n = 2$).

It is interesting to note that each exponential term in the former expressions gives the probability to overcome an energy barrier in a Boltzmann statistics either to bring a chain from the melt to the growth front or to create stable nuclei and induces a time lag before the crystallization starts. This time lag or induction time reflects the probability to create and grow a new crystal and increases when this event becomes unlikely. Experimentally, one can expect for the aforementioned reasons a U-shaped temperature dependence of the induction time and a bell-shaped temperature dependence for the overall crystallization kinetics and the nucleation rate.

Assuming the concentration of heterogeneities is constant over the temperature interval comprised between the initial melt temperature and the crystallization temperature, Ishida and Bussi[29] easily showed that the product of the nucleation rate, $N(T)$ times the induction time is constant. This result confirms the intuitive idea that the induction time is inversely proportional to the nucleation rate. For undercoolings such that the

critical size of stable nuclei is around unity or lower, the induction time is controlled by the nucleation step of the first row and is given by:

$$\tau_{\text{ind}} = \tau_{01} \exp\left(\frac{U^*}{R(T - T_0)}\right) \exp\left(\frac{16\sigma\sigma_e\Delta\sigma(T_m^0)^2}{k\Delta T^2 \Delta H_m^2}\right), \quad (6)$$

which is equivalent to the expression derived by Ishida and Bussi.[29]

From the crystallization kinetics, we will calculate the interfacial free energy $\Delta\sigma$. The temperature dependence of the induction time will be fitted with eq. (6) to calculate U^*, τ_{01}, and $\Delta\sigma$. From eq. (3), N will be calculated with the measured values of $t_{1/2}$ and G for different isothermal temperatures. Then, the temperature dependence of the nucleation rate $N(T)$ will be analyzed with eq. (4).

EXPERIMENTAL

Materials

A commercial grade of PLLA (Biomer L9000) with a weight-average molecular weight (M_w) of 220 × 10^3 g mol^{-1}, a number-average molecular weight (M_n) of 122 × 10^3 g mol^{-1}, and a polydispersity index (M_w/M_n) of 1.95 was purchased from Biomer, Krailling, Deutschland.

The alkylammonium-modified MMT and C30B were purchased from Southern Clay Product and used as received.

The pristine MMT, MMT, and MMT intercalated with selected seaweeds, named ALL350 in this study, were kindly supplied by Professor Jocelyne Miehe-Brendle from Ecole Nationale Supérieure de Chimie de Mulhouse.

The main organic modifier of ALL350 is a complex containing a polysaccharide, called ulvan, and glycoproteins extracted from the marine green alga *Ulva sp.* better known as sea lettuce. A review article, recently published by Lahaye and Robic,[30] documented the structure and the functional properties of Ulvan. Ulvan is a water-soluble anionic polysaccharide structurally heterogeneous containing sulfate, xylose, rhamnose, and glucuronic acid.[31,32]

The dosage of sugars for the polysaccharide and the glycoprotein expressed in percentage of dried matter carried out by Dr. Benjamin Saulnier from Institut National de la Recherche Agronomique (France) (Nantes) are resumed in Table I. The composites were obtained by mixing a water solution of clay with a water solution of polysaccharide–glycoprotein complex for 24 h at ambient temperature. The mixture was then centrifuged at 20,000 rpm for 10 min, and the solid was washed three times to remove the excess of organic matter physically adsorbed on the clay surface before being air dried. Keller et al.[33] determined the expansion of the (001) basal plane of the phillosilicate by X-ray diffraction. These authors showed that intercalation is partially obtained with a polysaccharide–glycoprotein complex: clay ratio of 5 : 1 (w/w) when the composites are air dried.

Preparation of PLA Nanocomposites

Natural clay and organomodified clays (powder form) and PLA (pellets) were dried under vacuum at 60°C for 48 h. The mixture containing 3% nanoclays was then melt extruded using a Brabender twin-screw extruder DSK 42/6 with three different zones operated, respectively, at 160, 180, and 180°C in the die. The screw speed was set at 60 rpm to obtain nanocomposite strands. Unfilled PLA was equally processed to obtain an unfilled reference with the same thermal processing history. Rheological specimens were prepared by hot pressing at 180°C for 4 min.

Table I. Composition of ALL350, Ulvan, and Glycoprotein Containing Sulfate, Xylose, Rhamnose, Glucuronic Acid, and Uronic Acid

	Rhamnose	Glucuronic acid	Xylose	Uronic acid
ALL350	3.3	4.8	0.7	4.7
Ulv	4.4	4.2	1.8	4.7
Prot	0.4	7.5	1.2	0.7

Transmission Electronic Microscopy

The nanoscale structure was investigated by means of transmission electron microscopy (TEM) (Philips XL300) operated at an acceleration voltage of 100 kV. The ultrathin section with a thickness of 100 nm was cut using a Richert cryoultramicrotome.

Polarized Optical Microscopy

Cross-polarization optical microscopy measurements were carried out on a LEICA apparatus equipped with a METTLER TOLEDO FP82HT hot stage and a video camera (JVC-TKC1381) and driven by Lida software. Specimens with a typical thickness of 100 μm were prepared by melt quenching between thin glass slides and further crystallized in the hot stage at the desired isothermal crystallization temperature.

Thermal Analysis

Isothermal crystallization studies and the glass transition temperature determination were performed on a Perkin-Elmer Pyris 1 Differential Scanning Calorimeter (DSC) under constant nitrogen flow. Temperature and heat of fusion were calibrated with an indium and zinc standards, respectively. Samples were heated from 25 to 190°C with a heating rate of 10°C min^{-1} and held for 5 min to eliminate any possible crystallinity or residual stress. Then, the specimens were rapidly quenched at 70°C min^{-1} to a desired isothermal crystallization temperature and held there until complete crystallization. Thus, samples were heated to 190°C at 10°C min^{-1} to probe the melting of the polymer and checked that no degradation occurred during the long-lasting crystallization kinetics.

Rheological Measurements

Rheological measurements were carried out on a Bohlin Gemini rheometer under a nitrogen atmosphere to avoid any thermal oxidation. Dynamic rheological measurements were performed at a fixed temperature of 180°C in oscillatory shear mode using a set of parallel plate geometry with a diameter of 25 and 2 mm thick samples. Frequency sweeps between 0.01 and 10 Hz were performed at low strain (5%), which was previously checked to be within the linear viscosity range. The time sweep tests at working temperature were also carried out to ensure no significant thermal degradation occurred within the experimental time.

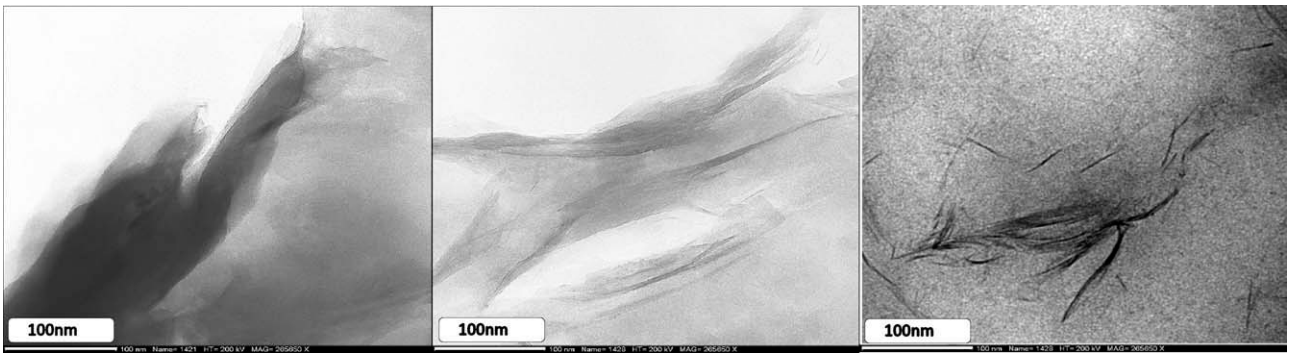

Figure 1. TEM images of PLLA/MMT, PLLA/ALL350, and PLLA/C30B (from left to right).

RESULTS AND DISCUSSION

The main incentive of this work is to study the nucleating effect of a MMT intercalated with a green algae biopolymer on the crystallization behavior of PLLA. The nucleating ability of green modified MMT (ALL350) is compared to those of C30B and pristine MMT. The properties of composites containing 3% (w/w) nanoclay were compared. Indeed, C30B and ALL350 are intercalated MMT and contain about 20% of organic material, quaternary ammonium for C30B and ulvan for ALL350.

In a first step, the exfoliation is followed both by TEM and rheological measurements that are highly sensitive to the dispersion state in the PLA matrix. Then, the cross-polarized optical microscopy is used to characterize the crystal morphology at several stages of crystallization. Subsequently, the overall isothermal crystallization rate and the induction time followed by DSC are analyzed and discussed to further gain insight on the promoting effect of the used fillers.

TEM micrographs of PLLA nanocomposites are shown in Figure 1. PLLA with natural MMT clearly exhibits large micrometric aggregates that demonstrate that no exfoliation takes place without any pretreatment of the filler before melt blending. ALL350 yields a more complex nanostructure for which some individual scattered platelets are observed, while large aggregates are evidenced as well. C30B yields the same nanostructure with quantitatively more individual platelets and less aggregates than for ALL350 systems.

To understand the effects of the organomodifier on the interfacial interactions between clay layers and polymer chains, the rheological behavior of neat PLLA and corresponding nanocomposites was compared. Dynamic frequency sweep tests were carried out to probe the extent of exfoliation of the different fillers. Figure 2 shows the frequency dependence of the storage modulus (G') for neat PLLA, PLLA/C30B, PLLA/MMT, and PLLA/ALL350.

Neat PLLA exhibits the classical rheological polymer melt behavior with a slope of G' versus frequency in a double logarithmic scale equals to 2. For PLLA/MMT, no modification of G' was observed especially at low frequencies compared with neat PLLA. These results evidence the poor cohesion of these systems and therefore underline a state of dispersion at a micrometric rather than a nanometric scale. This low dispersion is consistent with the observation on the TEM images. In the case of PLLA/C30B, G' is the highest in the entire range of frequencies studied. Especially at low frequencies, G' becomes less frequency dependent, which is characteristic of materials showing pseudo-solid-like behavior.[34] This behavior due to the formation of a physical network of clay layers at relatively low clay fractions has already been observed in nanocomposites[35] and is a proof of a partial or total exfoliation. The evolution of G' for PLLA/ALL350 is quite similar to PLLA/C30B but shifted down to lower values. This behavior will be discussed in the following sections.

It is thus possible to rank qualitatively the filler in terms of their dispersion in the matrix from a higher to a poorer dispersion: C30B, ALL 350, and natural MMT.

The evolutions of the dynamic viscosity, obtained from the frequency sweep tests, are shown in Figure 3. Neat PLLA shows, at low frequency, a Newtonian plateau, whereas PLLA/MMT presents only a slight increase compared with neat PLLA. This last point shows that the dynamic viscosity of the PLLA is not affected by 3% of natural clay without a compatibilizer. The highest complex viscosity is achieved with the C30B. It can be

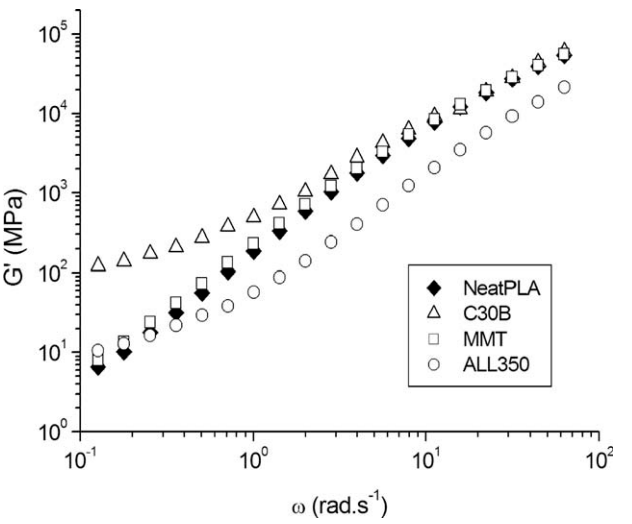

Figure 2. Frequency dependence of storage modulus (G') for neat PLLA, PLLA/C30B, PLLA/MMT, and PLLA/ALL350.

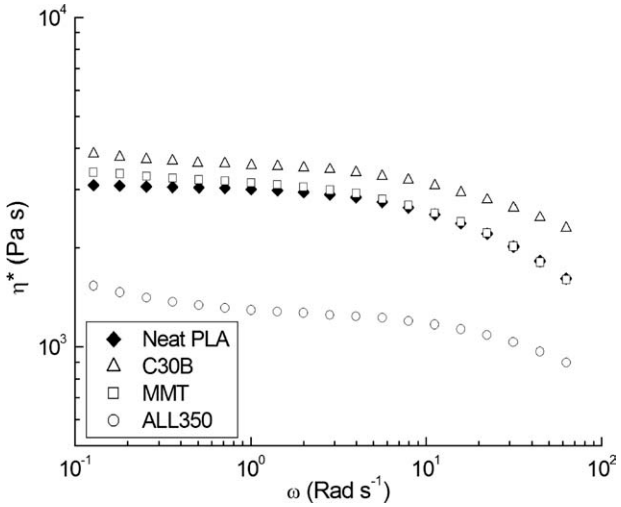

Figure 3. Frequency dependence on complex viscosity for neat PLLA, PLLA/C30B, PLLA/MMT, and PLLA/ALL350.

observed that η^* increases slightly at low frequency showing a shear thinning behavior. We assign this increase to a better dispersion of the filler and a possible compatibilizing effect of the Cloisite intercalated with the PLLA matrix. PLLA/ALL350 presents a behavior quite similar to PLLA/C30B but shifted to lower η^*, which is rather unexpected. As already mentioned in the Experimental section, we have checked, by gel permeation chromatography measurements, that no chain scissions occurs so that any degradation mechanism can be excluded to account for a decrease of η^*. This decrease of viscosity could be attributed to a plasticizing effect of sugar-like small molecules, which is commonly arising from degradation of the polysaccharide and the glycoprotein. This plasticizing effect of glucose (or other sugar-like small molecules) on PLLA has already been reported in literature.[36] However, no shift of neither the glass transition, T_g, nor the melting temperature, T_m, was registered in those systems. A possible explanation to account for this discrepancy is the small amount of sugar-like small molecules present in the system (around 18% of the organic content, thus

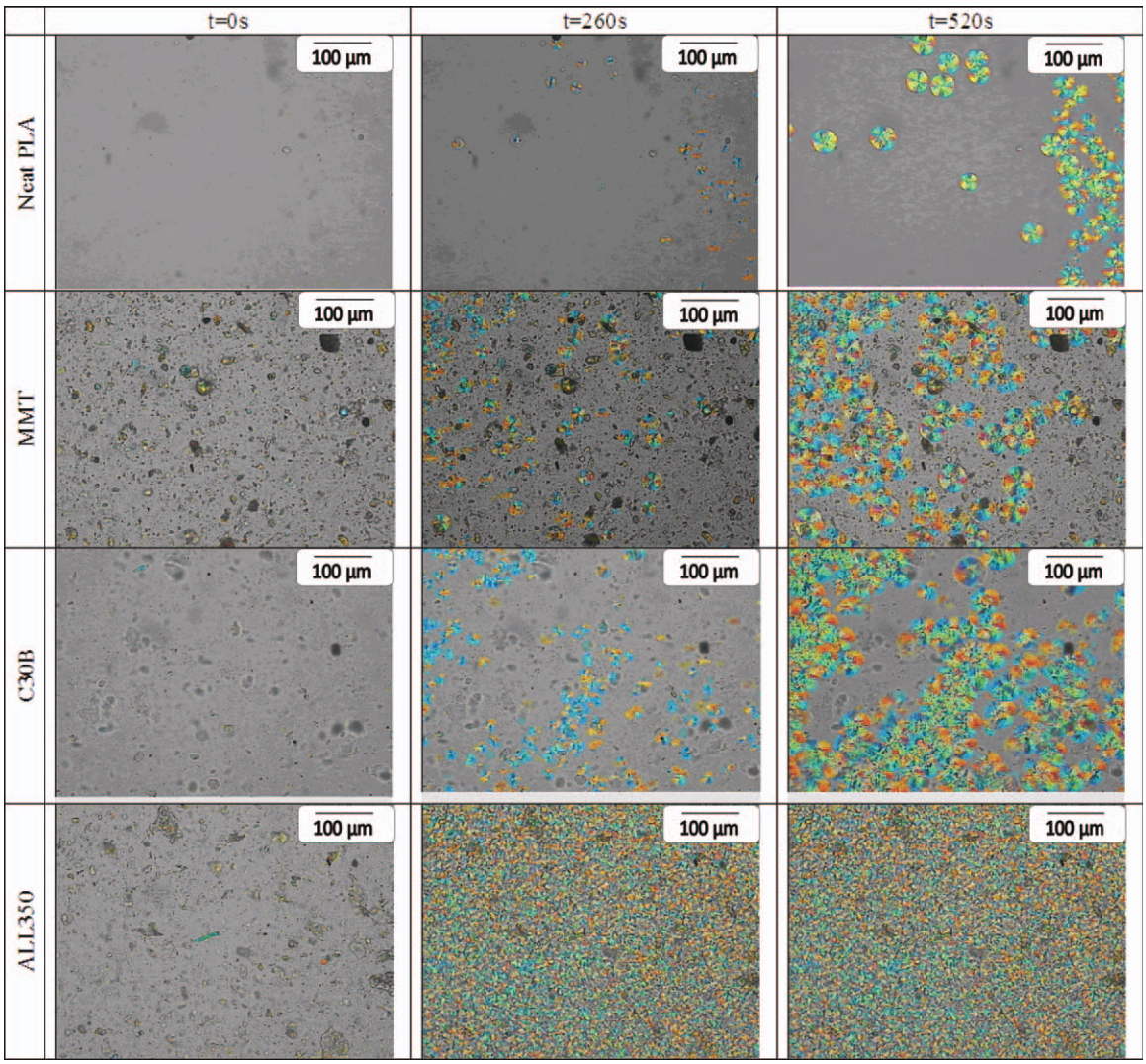

Figure 4. Cross-polarization optical microscope images of neat PLLA and corresponding nanocomposites at time zero and other two different stages. (The red scale bar indicates 50 μm). $T_c = 130°C$. [Color figure can be viewed in the online issue, which is available at wileyonlinelibrary.com.]

Table II. Avrami Exponent, n Values, at Different Crystallization Temperatures Obtained for Neat PLLA and Corresponding Nanocomposites

T_c (°C)	Neat PLLA	PLLA/ALL350	PLLA/MMT	PLLA/C30B
110	3.01	3.11	3.48	2.86
120	2.81	3.12	2.99	2.74
130	2.57	3.14	2.78	2.54
140	2.68	2.79	2.77	2.65

<0.5% of the total weight). What remains unclear is whether the drop of viscosity is due to an excess of ulvan or glycoprotein adsorbed on the surface of MMT that can desorb in the PLA melt.

Figure 4 represents the cross-polarization optical microscope images of neat PLLA and respective nanocomposites at two different stages (t = 260 and 520 s). At an early crystallization stage (Figure 4: $t_{0\ s}$) and an intermediate crystallization stage (Figure 4: $t_{260\ s}$), the crystal morphology of the neat PLLA, PLLA-MMT, PLLA-C30B, and PLLA-ALL350, respectively, is presented. For the neat PLLA and PLLA filled with natural MMT or C30B, it can be clearly seen that morphology appears circular, suggesting a three-dimensional spherulitic morphology. In the presence of ALL350, the crystal morphology is hard to determine because of the small spherulite size.

The presence of microaggregates of clay can be distinguished before the beginning of crystallization. The interesting feature is that for all the composite systems, the nucleation is not promoted at the vicinity of the aggregates but somewhere else in the matrix, where no trace of filler is detectable with the resolution of the optical microscope. This last point might be a clue to the dispersion of bundles of layers or of individual sheets and will be further discussed. In the case of neat PLLA, PLLA/MMT, and PLLA/C30B, the spherulite size, at the same elapsed time (t = 520 s) after the induction period, is similar, suggesting that crystal growth is not affected by the presence of the filler. This last point is better seen by measuring the growth rate of spherulites for the PLLA, PLLA-MMT, PLLA-C30B, and PLLA-ALL350 composites at 145°C. For each system, a linear crystal growth rate of 0.026 μm s^{-1} is measured for all the samples confirming the independence of the crystal growth rate on the filler presence.

To confirm and further understand the hypothesis concerning the heterogeneous nucleation mechanism and the lamellar morphology, isothermal crystallization kinetics for different undercoolings were realized by DSC. Samples were heated from 25 to 190°C with a heating rate of 10°C min^{-1} (stage 1) and held for 5 min to eliminate any possible crystallinity or residual stress. Then, the specimens were rapidly quenched at 70°C min^{-1} to a desired isothermal crystallization temperature and held there until complete crystallization. Thus, samples were heated to 190°C at 10°C min^{-1} to probe the melting of the polymer and checked that no degradation occurred during the long-lasting crystallization kinetics. Plotting eq. (3) as $\log(-\ln(1-\alpha))$ versus $\log(t)$ allows to determine that n (from the slope) and $\log(K)$ (from the intercept) witch are the Avrami exponent and the temperature-dependent rate constant, respectively. Avrami's law is rarely obeyed over the whole range of crystalline fractions but can fit the data pretty well over a limited range. Thus, limitation induces an experimental uncertainty on the Avrami exponent determination. The values of the Avrami exponent, n, for all the systems studied are reported in Table II. The n values close to 3 indicate three-dimensional crystalline entities and a heterogeneous nucleation mechanism that is in agreement with the microscopic analysis.

The half-time crystallization, for the different PLLA systems, shows a U-shaped temperature dependence (Figure 5). At higher undercoolings, two observations can be made. First, the maximum of the overall crystallization rate is reached at higher temperature in the case of PLLA–ALL350 compared with the neat PLLA and the other composite systems. Second, the overall crystallization time of PLLA is lowered when filler is added whatever its nature. This decrease of the crystallization kinetics is consistent with an increase of the dynamic viscosity, as noted in Figure 3, for the PLLA-MMT and PLLA-C30B systems. Following the same line of thought, we should observe a higher rate for PLLA–ALL350 system that is not the case. Thus, to account for this discrepancy, we have to infer that a decrease of the nucleation rate is at stake in this last case.

At low undercooling, the crystallization kinetics is controlled by the thermodynamic conditions to create a stable nucleus, whereas for higher undercooling, the transport of the chains from the melt to the growth front is the dominant mechanism. The nucleation and crystal growth are the result of these two competing antagonist mechanisms and go through a maximum when the crystallization temperature varies from the onset crystallization temperature to the glass transition temperature. In the thermodynamically controlled regime, it can be noted a strong enhancement of the overall crystallization kinetics by a factor 10 at 140°C when the ALL350 filler is added and an

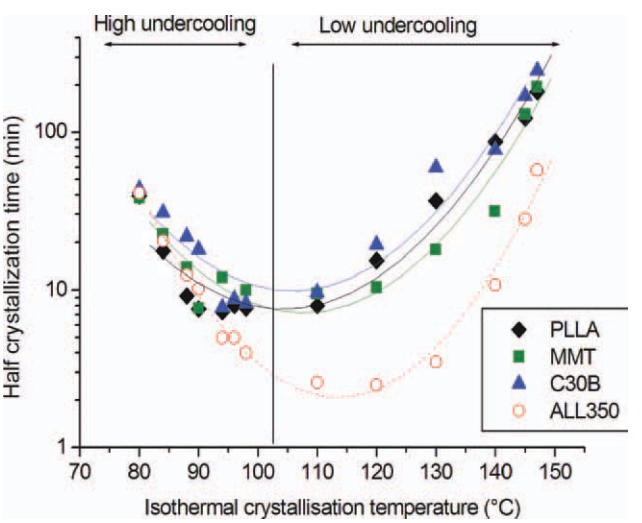

Figure 5. Half-time crystallization rate as a function of isothermal crystallization temperature for neat PLLA and corresponding nanocomposites. [Color figure can be viewed in the online issue, which is available at wileyonlinelibrary.com.]

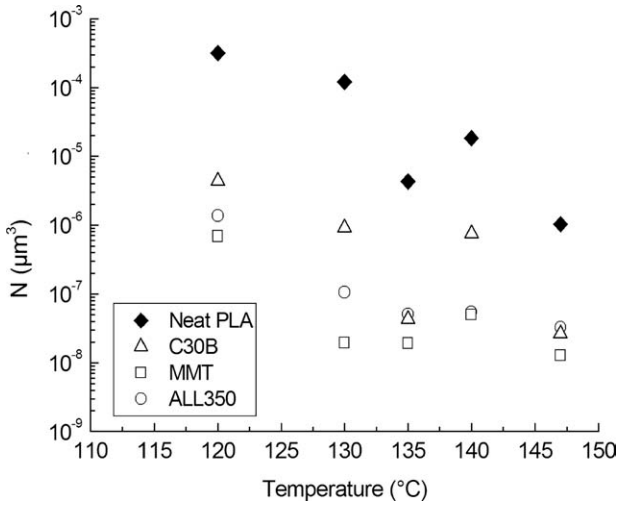

Figure 6. Influence of nanoclays on the overall nucleation rate of PLLA.

increase by a factor 2.8 at 140°C for the natural MMT. No significant modification of the overall crystallization rate is observed in the case of C30B. These results are consistent, on one hand, with an increase of the nucleation for a poor dispersion of natural clay in PLLA and with the absence of any effect of C30B on the crystallization of PLLA, on the other hand.[14]

Moreover, a discontinuity in the bell curve is observed in Figure 5 for neat PLA and MMT, C30B-filled PLA, as well at temperatures close to 95°C, whereas this discontinuity is not observed for ALL350 samples. Several workers[37–41] pointed out this effect for neat PLA just below 120°C. This phenomenon was ascribed to differences in polymorphic crystalline (α and α') form kinetics of crystallization. The difference in the discontinuity temperature for the PLLA used for our study is ascribed to its microstructure and molecular weight. There is a possible influence of the nanofiller nature on polymorphism of PLLA. Indeed, ALL350 suppresses the discontinuity in Figure 5 that could therefore yield an homogeneous crystalline phase.

As already concluded from the optical microscopy analysis, the addition of clay filler does not affect the linear growth rate (G). Thus, it is very likely that the strong modification of the crystallization kinetics is related to a change of the nucleation rate.

Equation (3) can be derived by assuming a perfect three-dimensional growth ($n = 3$) of the temperature dependence of the nucleation rate $N(T)$ according to:

$$N(T) = \frac{3Ln(2)}{4\pi}\left(\frac{1/t_{1/2}}{G(T)}\right)^3. \quad (3)$$

To calculate $N(T)$, the determination of the temperature dependence of the linear growth rate (G), G values for the neat PLLA were measured by optical microscopy. After data treatment using eq. (5), K_g and G_0 can be calculated and give values of 274,500 K^2 and 365 cm s^{-1}, respectively.

$N(T)$ values for the different systems applying the eq. (3′) were calculated using $1/t_{1/2}$ values and are plotted in Figure 6. The results are completely in agreement with the conclusion inferred from the analysis of the overall crystallization rate and the optical analysis. In the case of neat PLLA, the values found have the same order of magnitude of those reported by Nam et al. for a PLLA of a similar grade.[11]

To verify if the method used allows determining a correct order of magnitude of N, we have estimated N by direct observation from the polarized microscopy images. The number of spherulites in the PLLA/MMT and the PLLA/ALL350 was counted using the images reported in Figure 7. The results, reported in Table III, are in agreement with the calculated values.

Information on the nucleation rate can also be gained from the analysis of the temperature dependence of the induction period as shown in Figure 8. It appears clearly that the addition of ALL350 strongly shortens the induction period for isothermal crystallization temperatures higher than 94°C (the induction period represents the time when 5% of the total crystallinity is achieved). For the other fillers, their influence can be better

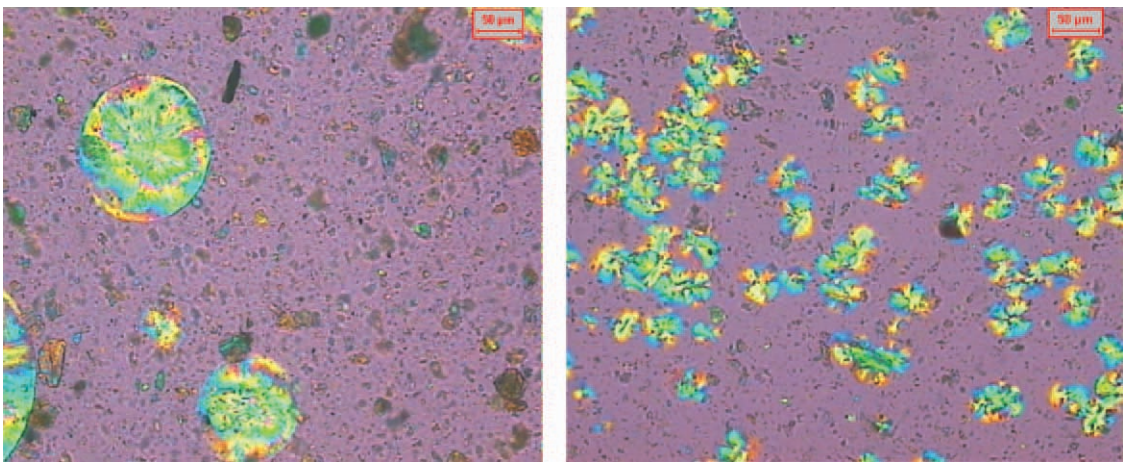

Figure 7. Cross-polarization optical microscope images of PLLA/MMT (left) and PLLA/ALL350 (right) at 145°C. (The red scale bar indicates 50 μm). [Color figure can be viewed in the online issue, which is available at wileyonlinelibrary.com.]

Table III. Comparison of $N(T)$ Values Obtained by Directed Estimation on Optical Microscopy Images and from Calculation Through eq. (3′)

	Spherulite number	Volume (μm^3)	N(145°C) estimated	N(145°C) calculated from eq. (3′)
PLLA/MMT	2	31.6×10^3	6.3×10^{-8}	7.7×10^{-8}
PLLA/ALL350	72	14.3×10^3	5.0×10^{-3}	4.7×10^{-8}

visualized by plotting the induction time normalized with respect to the PLLA induction time as shown in the insert of Figure 8. This result let us suppose that when the crystallization is obtained from the melt (with high mobility of PLA chains), the first crystals of PLA on ALL350 nanoparticles have stability better than with the other fillers. The U-shaped temperature dependence is well obeyed.

One interesting finding in this work is the diversity of the observed behaviors compared with the statement reported by Pochan and coworker[14] concerning the poor nucleation ability of clay nanofiller when it is well dispersed in a PLLA matrix. This experimental observation seems to be contradicted by the intercalation of an ulvan–glycoprotein complex in a natural MMT. Several experimental evidences suggest that some layers of ALL350 are dispersed in the PLLA matrix although it is undeniable from the presence of the macroaggregates that the dispersion is rather incomplete. The presence of some scattered platelets on TEM images is confirmed by the increase of the storage modulus in the low frequency region advocating for the creation of a physical network. Moreover, the decrease of the complex viscosity that has been related to the dispersion of the ulvan–glycoprotein complex in PLLA matrix shows that some exfoliation occurs.

In relation to the modification of the viscosity, one can wonder if the promoting effect of ALL 350 on the nucleation rate is due to the dispersion in the matrix of the ulvan–glycoprotein complex, or if some layers embedded in the biopolymers are exfoliated and act as a nucleating agent. A partial answer to this issue can be found by analyzing the induction time of PLLA when the neat ulvan or glycoprotein contained in the green algae is added separately or intercalated in the MMT clay. From the results presented in Figure 8, it can be concluded that the addition of neither ulvan nor glycoprotein enhanced the nucleation rate. On the other hand, at low undercoolings, the induction time is shortened by a factor of three to four in the presence of MMT intercalated either with ulvan or the glycoprotein. In the diffusion-controlled regime, the differences are not significant enough according to the dispersion of the results to draw any conclusion on the impact of the biomontmorillonite on the diffusion.

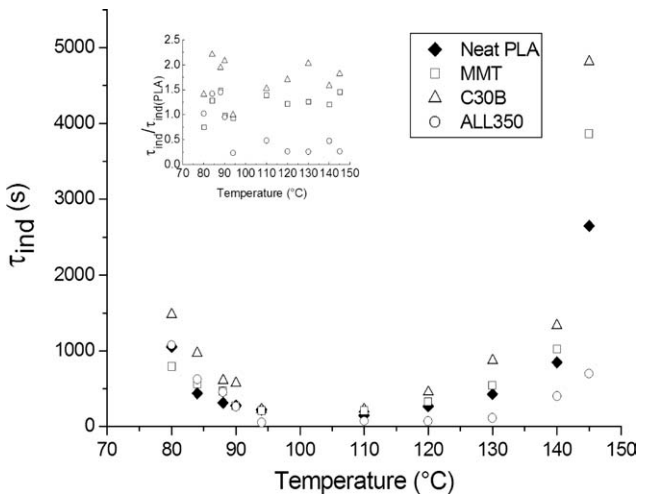

Figure 8. Induction time as a function of T_c for neat PLLA and corresponding nanocomposites.

Concerning the nucleation ability, a determinant parameter seems to be the interfacial energy difference $\Delta\sigma$ that governs the height of the thermodynamic energy barrier as shown in eq. (4). We determine hereafter this parameter from the crystallization kinetics by one of the methods presented in the background part. The temperature dependence of the induction time shown in Figure 8 is fitted with eq. (6) to calculate the thermodynamic activation energy $K_1 = \left(\frac{16\sigma\sigma_e\Delta\sigma(T_m^0)^2}{k\Delta H_m^2}\right)$.

Using the value obtained for K_g, the lateral surface free energy, σ, and the free energy of folding, σ_e, can be calculated. The values of $\sigma\sigma_e$ are calculated from the parameters given above assuming a growth regime II and $\sigma\sigma_e = 8.5 \times 10^{-4}$ J^2 m^{-4}, which agrees well with other results given in the literature.[42] Using $\sigma\sigma_e$ value, we reported the obtained values of $\Delta\sigma$ in Table IV.

The values of $\Delta\sigma$ are on the order of magnitude of 10^{-4} J m^{-2} and are comparable with $\Delta\sigma$ values found for other systems.[43] In a first time, it can be observed similar values of $\Delta\sigma$ for PLLA, C30B, and MMT. A decrease about 20% is observed for ALL350. These results seem to indicate a better nucleation rate when the interfacial tension decreases.

To estimate the single free surface energies σ and σ_e, the empirical Thomas–Staveley equation can be used[44]:

$$\sigma = \alpha(\Delta H_m^0)(a_0 b_0)^{1/2}, \quad (7)$$

where α is an empirical constant calculated by Hoffman et al.[45] and Di Lorenzo and Righetti[46] for polyester of 0.23. The unit parameter cell, $a_0 = 1.08$ nm and $b_0 = 0.62$ nm, was determined by Miyata and Masuko[47] and Wasanasuk and Tashiro[48] for PLLA in orthorhombic form (α form) and $\Delta H_m^0 = 174 \times 10^6$ J m^{-3}.[47]

Table IV. Influence of Nanoclays on the Interfacial Energy

	Neat PLLA	PLLA/ C30B	PLLA/ MMT	PLLA/ ALL350
$K_l \times 10^{-4}$ (K^3)	1158	1168	1106	961
$\Delta\sigma \times 10^{-4}$ (J m^{-2})	6.4	6.5	6.1	5.3

σ value was then calculated as 24×10^{-3} J m^{-2} and σ_e as 35×10^{-3} J m^{-2}. These results are comparable to those obtained for PLA.[42,47,49]

CONCLUSIONS

We showed that the intercalation of MMT with an ulvan–glycoprotein complex extracted from a green alga turns out to be an effective nucleating agent of PLLA. It was also showed that this bioorganic modifier decreases the complex viscosity. We ascribe this behavior to a plasticizing effect due to the glucose contained in the ulvan and the glycoprotein.

The comparison of the ALL 350 nucleation ability with that of the polysaccharide or the glycoprotein clearly showed that the crystals are nucleated at the surface of exfoliated layers. When added to the PLLA matrix, the overall crystallization kinetics is faster because of a shortening of the induction time and a dramatic enhancement of the nucleation rate. We ascribed this nucleation effect to the lowering of the interfacial energy. Moreover, ALL350 suppresses the discontinuity in the bell curve that yields a more homogeneous resulting crystalline phase. Similar effects, but to a lower extent, were observed with natural clay, whereas no significant change was noted when C30B is added.

ACKNOWLEDGMENTS

The authors thank the FEDER European program, the Brittany region, and the French Ministry of Research for their financial support. Moreover, the NanoFunc program and especially O. Chauvet and N. Gautier from the IMN are greatly acknowledged.

REFERENCES

1. Sinha Ray, S.; Bousmina, M. *Prog. Mater. Sci.* **2005,** *50*, 962.
2. Nam, J. Y.; Sinha Ray, S.; Okamoto, M. *Macromolecules* **2003,** *36*, 7126.
3. MacDonald, R. T.; McCarthy, S. P.; Gross, R. A. *Macromolecules* **1996,** *29*, 7356.
4. Tsuji, H.; Mizuno, A.; Ikada, Y. *J. Appl. Polym. Sci.* **2000,** *77*, 1452.
5. Schmidt, S. C.; Hillmyer, M. A. *J. Polym. Sci. Part B: Polym. Phys.* **2001,** *39*, 300.
6. Urayama, H.; Kanamori, T.; Fukushima, K.; Kimura, Y. *Polymer* **2003,** *44*, 5635.
7. Tsuji, H. *Macromol. Biosci.* **2005,** *5*, 569.
8. Brochu, S.; Prud'homme, R. E.; Barakat, I.; Jerome, R. *Macromolecules* **1995,** *28*, 5230.
9. Kolstad, J. J. *J. Appl. Polym. Sci.* **1996,** *62*, 1079.
10. Zhang, J.-F.; Sun, X. *Polym. Int.* **2004,** *53*, 716.
11. Nam, P. H.; Ninomiya, N.; Fujimori, A.; Masuko, T. *Polym. Eng. Sci.* **2006,** *46*, 39.
12. Sinha Ray, S.; Okamoto, K.; Okamoto, M. *Macromolecules* **2003,** *36*, 2355.
13. Krikorian, V.; Pochan, D. *J. Chem. Mater.* **2003,** *15*, 4317.
14. Krikorian, V.; Pochan, D. J. *Macromolecules* **2004,** *37*, 6480.
15. Ke, T.; Sun, S. X.; Seib, P. *J. Appl. Polym. Sci.* **2003,** *89*, 3639.
16. Darder, M.; Colilla, M.; Ruiz-Hitzky, E. *Chem. Mater.* **2003,** *15*, 3774.
17. Wang, S. F.; Shen, L.; Tong, Y. J.; Chen, L.; Phang, I. Y.; Lim, P. Q.; Liu, T. X. *Polym. Degrad. Stab.* **2005,** *90*, 123.
18. Wu, T.-M.; Wu, C.-Y. *Polym. Degrad. Stab.* **2006,** *91*, 2198.
19. Tsuji, H.; Takai, H.; Fukuda, N.; Takikawa, H. *Macromol. Mater. Eng.* **2006,** *291*, 325.
20. Hoffman, J. D. *Polymer* **1983,** *24*, 3.
21. Johnson, W. A.; Melh, R. F. *Trans. Am. Inst. Min. Eng.* **1939,** *135*, 416.
22. Avrami, M. *J. Chem. Phys.* **1939,** *7*, 1103.
23. Avrami, M. *J. Chem. Phys.* **1940,** *8*, 212.
24. Avrami, M. *J. Chem. Phys.* **1941,** *9*, 177.
25. Kolmogorov, A. N. *Acad. Sci. USSR* **1937,** *3*, 355.
26. Turnbull, D.; Fisher, J. C. *J. Chem. Phys.* **1949,** *17*, 71.
27. Lauritzen, J. I.; Hoffman, J. D. *J. Res. Natl. Bur. Stand. Sect. A* **1961,** *65*, 297.
28. Hoffman, J. D.; Frolen, L. J.; Ross, G. S.; Lauritzen, J. J. I. *J. Res. Natl. Bur. Stand. Sect. A* **1975,** *79*, 671.
29. Ishida, H.; Bussi, P. *Macromolecules* **1991,** *24*, 3569.
30. Lahaye, M.; Robic, A. *Biomacromolecules* **2007,** *8*, 1765.
31. Brading, J. W. E.; Georg-Plant, M. M. T.; Hardy, D. M. *J. Chem. Soc.* **1954,** 319.
32. McKinnel, J. P.; Percival, E. *J. Chem. Soc.* **1962,** 2082.
33. Keller, L.; Decker, C.; Zahouily, K.; Benfarhi, S.; Le Meins, J. M.; Miehe-Brendle, J. *Polymer* **2004,** *45*, 7437.
34. Sinha Ray, S.; Okamoto, M. *Macromol. Rapid Commun.* **2003,** *24*, 815.
35. Di, Y.; Iannace, S.; Di Maio, E.; Nicolais, L. *J. Polym. Sci. Part B: Polym. Phys.* **2005,** *43*, 689.
36. Jacobsen, S.; Fritz, H. G. *Polym. Eng. Sci.* **1999,** *39*, 1303.
37. Kawai, T.; Rahman, N.; Matsuba, G.; Nishida, K.; Kanaya, T.; Nakano, M.; Okamoto, H.; Kawada, J.; Usuki, A.; Honma, N.; Nakajima, K.; Matsuda, M. *Macromolecules* **2007,** *40*, 9463.
38. Di Lorenzo, M. L. *Eur. Polym. J.* **2005,** *41*, 569.
39. Pan, P.; Inoue, Y. *Prog. Polym. Sci.* **2009,** *34*, 605.
40. Di Lorenzo, M. L.; Cocca, M.; Malinconico, M. *Thermochim. Acta* **2011,** *522*, 110.
41. Pan, P.; Zhu, B.; Kai, W.; Dong, T.; Inoue, Y. *J. Appl. Polym. Sci.* **2008,** *107*, 54.
42. Miyata, T.; Masuko, T. *Polymer* **1998,** *39*, 5515.
43. Muchová, M.; Lednický, F. *Polymer* **1996,** *37*, 3031.
44. John, I.; Lauritzen, J.; Hoffman, J. D. *J. Appl. Phys.* **1973,** *44*, 4340.
45. Hoffman, J. D.; Miller, R. L.; Marand, H.; Roitman, D. B. *Macromolecules* **1992,** *25*, 2221.
46. Di Lorenzo, M. L.; Righetti, M. C. *Polym. Eng. Sci.* **2003,** *43*, 1889.
47. Miyata, T.; Masuko, T. *Polymer* **1997,** *38*, 4003.
48. Wasanasuk, K.; Tashiro, K. *Polymer* **2011,** *52*, 6097.
49. Garlotta, D. *J. Polym. Environ.* **2001,** *9*, 63.